Front-End Parameter Identification Method Based on Adam-W Optimization Algorithm for Underwater Wireless Power Transfer System

Bo Luo, *Senior Member, IEEE*, Huan Wu, Mengyao Wang, Fangrui Wang, Longlei Bai, Chaoqiang Jiang, *Senior Member, IEEE*, and Jiang You, *Member, IEEE*

***Abstract*—Monitoring coupler parameters in underwater wireless power transfer (UWPT) systems is crucial for improving the system transmission characteristics. Due to the eddy current effect, the equivalent circuits of the magnetic coupler are more complex and contain more parameters than those in air-based circuits. Traditional parameter identification methods, which rely on solving circuit matrix equations, often struggle with the complex UWPT systems or require significant computational resources to solve high-order multivariate equations. This article proposes a coupler parameter identification method based on the adaptive moment estimation with a weighted adjustment (Adam-W) optimization algorithm to address the multiparameter identification problems in the UWPT system. This method transforms the problem of solving high-order matrix equations into an optimization problem to address multiparameter identification problem caused by seawater eddy effect, which is challenging for traditional methods. In addition, it facilitates online monitoring of the characteristic parameters of the system's coupler by detecting the system's front-end input current and voltage without wireless communication and additional sensor modules, and exhibits better reliability in underwater environments. The experimental results show that the proposed Adam-W algorithm achieves a high parameter identification accuracy within 1 s and 94 iterations with an average error of 2.78%. Comparably, an average error of 56.74% is achieved by gradient descent and 41.49% by adaptive moment estimation, and 37.42% by particle swarm optimization in 150 iterations. The proposed Adam-W algorithm achieves higher accuracy in parameter identification of the UWPT system within a shorter time and demonstrates better applicability in seawater environments.**

***Index Terms*—Adaptive moment estimation (Adam), coupler parameter identification, gradient descent (GD), inductive power transfer (IPT), optimization algorithm, underwater wireless power transfer (UWPT).**

I. Introduction

AUTONOMOUS underwater vehicles (AUVs) are vital for studying marine ecosystems and exploring marine environmental resources [1], [2], [3], [4]. However, energy limitations restrict their operational duration. Currently, AUVs mainly rely on surface vessels, platforms, or nearshore cables to obtain energy, which compromises safety, concealment, and automation [5], [6], [7]. Wireless power transfer (WPT) offers a promising solution to these energy transmission challenges, providing enhanced flexibility, reliability, and stability [8], [9]. WPT includes magnetic field coupling, electric field coupling, and other methods [10], [11], [12], [13]. Especially, inductive power transfer (IPT) based on the magnetic coupling is usually used in short- and medium-distance power transmission to AUVs [14].

However, the conductive nature of seawater introduces complex eddy current effects in the IPT system, increasing transmission losses [15], [16]. In addition, underwater dark waves can displace the coupling coils, causing unpredictable changes in the coupling parameters and deviating the system from optimal operation. Therefore, online monitoring for identifying the underwater wireless power transfer (UWPT) system's coupler parameters is crucial for researching the system characteristics, refining system control strategies, and enhancing the stability and efficiency [17], [18], [19].

Existing parameter identification methods are mainly categorized into analytical, data-driven, and system model methods. The analytical model method directly solves equations derived from circuit structure or transfer functions. For example, Yin et al. [20], [21] identified multiple load resistances of the WPT system by solving circuit matrix equations, while Zeng et al. [22] used additional current phase detection sensors on the primary side for rapid estimation of the coupling coefficient and resonance frequency. In addition, dynamical tracking of the mutual inductance coefficient is also proposed to improve transmission efficiency in [23], [24], and [25] based on the analytical method. However, these methods require the bilateral communication modules or other additional hardware, limiting

Received 17 June 2024; revised 28 August 2024 and 27 October 2024; accepted 15 November 2024. Date of publication 12 December 2024; date of current version 28 January 2025. This work was supported in part by the National Natural Science Foundation of China under Grant 52307006 and in part by the Fundamental Research Funds for the Central Universities under Grant 3072024GH2702. Recommended for publication by Associate Editor J. Acero. *(Corresponding author: Longlei Bai.)*

Bo Luo, Huan Wu, Mengyao Wang, Longlei Bai, and Jiang You are with the Yantai Research Institute, Harbin Engineering University, Yantai 264000, China (e-mail: longlei0107@hrbeu.edu.cn).

Fangrui Wang is with the College of Intelligent System Science and Engineering, Harbin Engineering University, Harbin 150001, China.

Chaoqiang Jiang is with the Department of Electrical Engineering, City University of Hong Kong,, Hong Kong.

Color versions of one or more figures in this article are available at https://doi.org/10.1109/TPEL.2024.3516493.

Digital Object Identifier 10.1109/TPEL.2024.3516493

their applicability to complex models. The analytical modeling method is effective for simple circuit models with few parameters. However, complex models often need additional prior knowledge or hardware support, and solving high-order multivariate equation for multiple parameters is challenging.

Data-driven methods, such as back propagation (BP) neural networks, treat the circuit system as a closed box, finding functional relationship between output features and the parameters. Mohagheghi et al. [26] used neural networks to establish the relationship between the input and output of a full-bridge diode rectifier, enabling real-time monitoring of system parameters. Su et al. [27] applied TensorFlow neural networks to identify the load and mutual inductance of a double-*LCC* compensated WPT system. However, these methods suffer from poor interpretability and require extensive data to create datasets for training neural networks, posing challenges for practical implementation [28].

System modeling methods combine analytical and data-driven method, using the existing typical system models in conjunction with optimization algorithms to analyze parameter values. For instance, a genetic algorithm was used for the online identification of seven characteristic parameters, including capacitance and inductance in dc/dc converters for fault diagnosis in [29]. A two-layer adaptive differential evolution algorithm for identifying parameters, such as self-inductance, mutual inductance, and load resistance in WPT systems based on SS resonant topology, is proposed in [30]. However, heuristic optimization algorithms lack interpretability and reliability in the identification process [31].

Although some works have been made in identifying WPT system parameters in air, applying these methods to UWPT systems presents several challenges. The traditional analytical model struggles with multiparameter identification due to seawater eddy effects, and hardware modules, such as sensors and communication, face limitations [20], [21], [22], [23], [24], [25]. In addition, the data-driven method encounters difficulties in data collection and shows poor model stability under complex seawater conditions [26], [27], [28]. Moreover, the system model method effectively addresses multiparameter identification issues, but heuristic optimization algorithms have slower identification speeds, taking several minutes [29], [30], [31].

Gradient descent (GD) offers better convergence, faster convergence speed, and greater interpretability compared with heuristic optimization algorithms [32], but easy to get trapped in local optimal solutions [33]. The adaptive moment estimation (Adam) algorithm improves upon GD by introducing momentum and adaptive learning rates, providing better robustness and anti-interference capabilities [34].

This article applies the Adam algorithm to the parameter identification in the UWPT system and introduces a weight parameter based on the structural characteristics of the parameter identification model, thereby improving the Adam algorithm into the Adam with a weighted adjustment (Adam-W) algorithm to enhance the accuracy of multiparameter identification. The contributions of this article include the following.

1) This article proposes a multiparameter identification method for WPT systems in underwater environments, based on the Adam-W optimization algorithm. By constructing an objective function, the multiparameter identification problem is transformed into an optimization problem, which effectively addresses the identification challenges posed by the seawater eddy effects in UWPT systems.
2) The article simplifies the equivalent model for eddy effects in UWPT systems, reducing the number of parameters that need to be identified and thereby decreasing the difficulty of parameter identification for UWPT systems.
3) The method employed in this study facilitates online multiparameter identification by collecting the single-port impedance values of the UWPT system, eliminating the need for bilateral communication or additional sensor modules, which avoids issues related to communication delays and interference in marine environments. In addition, it demonstrates better stability and identification speed compared with heuristic optimization algorithms, offering improved handling of coil displacement issues caused by underwater currents.
4) An experimental platform was established to validate the effectiveness of the proposed method in underwater environments. The performance of the proposed method was compared with particle swarm optimization (PSO), GD, and Adam algorithms under experimental conditions simulating underwater currents and varying salinity levels to verify the advantages and limitations of different algorithms.

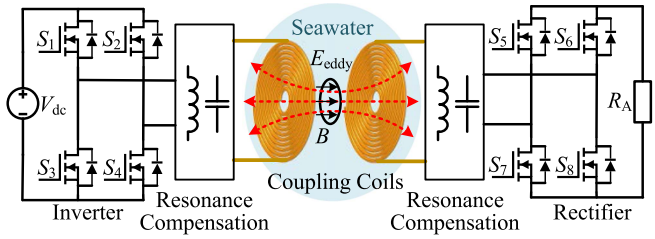

Fig. 1. Structural diagram of UWPT system.

II. Analysis of Circuit Models for UWPT System

The UWPT system mainly consists of an inverter, primary-side resonant compensation, coupled coils, secondary-side resonant compensation, and rectifier, with the coupled coils positioned in seawater, as shown in Fig. 1.

Due to the conductive nature of seawater, the UWPT system experiences complex eddy current effects in a marine environment. Therefore, the circuit model of the UWPT system needs to incorporate an eddy current loop with internal resistance, in addition to the air environment model [35]. Combined with the *SS* resonance compensation topology, the circuit model of the UWPT system is shown in Fig. 2.

At the transmitter, a full-bridge inverter with four MOSFETs (S_1–S_4) controlled by pulsewidth modulation (PWM) signals converts the dc input voltage V_{dc} into high-frequency ac input

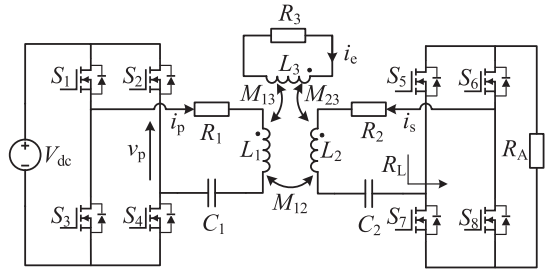

Fig. 2. Schematic diagram of UWPT system circuit based on *SS* resonance compensation.

voltage v_p. At the receiver, a full-bridge rectifier with four MOSFETs (S_5–S_8) converts the high-frequency ac voltage into dc voltage to power the load resistor R_A. R_1 and R_2 are the internal resistances of the transmitting coil and receiving coil in air, respectively; L_1 and L_2 are the self-inductances of the transmitting coil and receiving coil in air, respectively; R_3 is the equivalent impedance in the eddy current loop; L_3 is the equivalent self-inductance in the eddy current loop; M_{12} is the mutual inductance between the transmitting coil and receiving coil in the air; M_{13} and M_{23} are the equivalent mutual inductances among the transmitting coil, receiving coil, and eddy current loop; C_1 and C_2 are the resonant compensation capacitors; and i_p, i_s, and i_e represent the ac currents at the transmitting end, receiving end, and in the eddy current loop, respectively.

The fundamental components of the input voltage v_p, input current i_p, loop current i_s, and eddy current loop current i_e are denoted as v_{p1}, i_{p1}, i_{s1}, and i_{e1}, respectively. Under fundamental working frequency, the equivalent load resistance R_L can be calculated as follows:

$$R_L = \left(8/\pi^2\right) R_A. \tag{1}$$

After introducing the eddy current loop, the UWPT system's identification model becomes more complex, with more parameters to be identified, complicating the identification process. To simplify the coupler model, this article maps the equivalent parameters of the eddy current loop to the coupling coil. Based on Kirchhoff's voltage law (KVL), the following equations can be derived:

$$\begin{cases} v_{p1} = \left(j\omega L_1 + R_1 + \frac{1}{j\omega C_1}\right) i_{p1} + j\omega M_{12} i_{s1} + j\omega M_{13} i_{e1} \\ 0 = j\omega M_{13} i_{p1} + j\omega M_{23} i_{s1} + \left(R_3 + j\omega L_3\right) i_{e1} \\ 0 = \left(j\omega L_2 + R_2 + R_L + \frac{1}{j\omega C_2}\right) i_{s1} + j\omega M_{12} i_{p1} \\ \qquad\qquad + j\omega M_{23} i_{e1}. \end{cases} \tag{2}$$

Therefore, i_{e1} can be obtained as follows:

$$i_{e1} = \frac{j\omega M_{23} i_{s1} - j\omega M_{13} i_{p1}}{R_3 + j\omega L_3}. \tag{3}$$

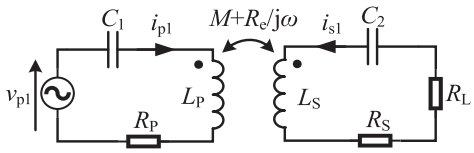

Fig. 3. Simplified UWPT system circuit.

By substituting (3) into (2) to eliminate the eddy current loop current i_{e1}, we simplify and obtain the following:

$$\begin{cases} v_{p1} = \begin{bmatrix} \left(R_1 + \frac{R_3\omega^2 M_{13}^2}{R_3^2+\omega^2 L_3^2}\right) + \frac{1}{j\omega C_1} \\ +j\omega\left(L_1 - \frac{L_3\omega^2 M_{13}^2}{R_3^2+\omega^2 L_3^2}\right) \end{bmatrix} i_{p1} \\ \qquad + \begin{bmatrix} \frac{R_3\omega^2 M_{13} M_{23}}{R_3^2+\omega^2 L_3^2} \\ +j\omega\left(M_{12} - \frac{L_3\omega^2 M_{13} M_{23}}{R_3^2+\omega^2 L_3^2}\right) \end{bmatrix} i_{s1} \\ 0 = \begin{bmatrix} \frac{R_3\omega^2 M_{13} M_{23}}{R_3^2+\omega^2 L_3^2} \\ +j\omega\left(M_{12} - \frac{L_3\omega^2 M_{13} M_{23}}{R_3^2+\omega^2 L_3^2}\right) \end{bmatrix} i_{p1} \\ \qquad + \begin{bmatrix} \left(R_2 + R_L + \frac{R_3\omega^2 M_{13}^2}{R_3^2+\omega^2 L_3^2} + \frac{1}{j\omega C_2}\right. \\ \left. +j\omega\left(L_2 - \frac{L_3\omega^2 M_{13}^2}{R_3^2+\omega^2 L_3^2}\right)\right) \end{bmatrix} i_{s1}. \end{cases} \tag{4}$$

According to (4), the simplified circuit model of the UWPT system is shown in Fig. 3.

The KVL equation for the circuit in Fig. 2 is simplified as follows:

$$\begin{cases} v_{p1} = \left(R_P + j\omega L_P + \frac{1}{j\omega C_1}\right) i_{p1} + \left(R_e + j\omega M\right) i_{s1} \\ 0 = \left(R_e + j\omega M\right) i_{p1} + \left(R_S + j\omega L_S + R_L + \frac{1}{j\omega C_2}\right) i_{s1}. \end{cases} \tag{5}$$

The equivalent relationship between the parameters of the UWPT system circuit model, including the eddy current loop, is shown as follows:

$$\begin{cases} R_P = R_1 + \frac{R_3\omega^2 {M_{13}}^2}{{R_3}^2+(\omega L_3)^2} \\ R_S = R_2 + \frac{R_3\omega^2 {M_{23}}^2}{{R_3}^2+(\omega L_3)^2} \\ L_P = L_1 - \frac{L_3\omega^2 M_{13}^2}{R_3^2+(\omega L_3)^2} \\ L_S = L_2 - \frac{L_3\omega^2 {M_{23}}^2}{{R_3}^2+(\omega L_3)^2} \\ R_e = \frac{R_3\omega^2 M_{13} M_{23}}{R_3^2+(\omega L_3)^2} \\ M = M_{12} - \frac{L_3\omega^2 M_{13} M_{23}}{{R_3}^2+(\omega L_3)^2} \end{cases} \tag{6}$$

where R_P and R_S represent the equivalent internal resistances of the simplified transmitting and receiving coils, respectively; L_P and L_S represent the equivalent inductances of the simplified transmitting and receiving coils, respectively; M represents the equivalent mutual inductance between the simplified transmitting and receiving coils; R_e represents the new equivalent parameter that represents the eddy current effect, defined as the mutual impedance of the eddy current effect. The parameters that need to be identified for the coupler include R_P, R_S, L_P, L_S, M, and R_e.

III. Parameter Identification Method Based on Optimization Adam-W Algorithms

A. Parameter Identification Model Establishment

The measured values of the transmission port impedance at the front end of the UWPT system at frequencies ω_k are denoted as $\hat{Z}(j\omega_k)$, which is calculated based on i_p and v_p obtained from sensors' measurements. $\hat{R}(j\omega_k)$ and $\hat{X}(j\omega_k)$ represent the real part and the imaginary part of the impedance measurement value $\hat{Z}(j\omega_k)$, respectively

$$\hat{Z}(j\omega_k) = \hat{R}(j\omega_k) + j\hat{X}(j\omega_k), k = 1, 2, \ldots, m. \tag{7}$$

The calculated values of the transmission port impedance at ω_k, based on the parameters to be identified, are denoted as $Z(j\omega_k)$, which is calculated from the KVL equation with unidentified parameters. $R(j\omega_k)$ and $X(j\omega_k)$ represent the real part and the imaginary part of the impedance calculated value $Z(j\omega_k)$, respectively

$$Z(j\omega_k) = R(j\omega_k) + jX(j\omega_k), k = 1, 2, \ldots, m. \tag{8}$$

$Z(j\omega_k)$ is a complex function composed of the parameters to be identified R_P, R_S, R_e, L_P, L_S, and M. According to (5), the specific expression for $Z(j\omega_k)$ is given as follows:

$$\begin{aligned} Z(j\omega_k) &= f(R_P, R_S, R_e, L_P, L_S, M, \omega_k) \\ &= \frac{1}{j\omega_k C_1} + j\omega_k L_P + R_p \\ &\quad - \frac{(j\omega_k M + R_e)^2}{\frac{1}{j\omega_k C_2} + j\omega_k L_s + R_L + R_s}. \end{aligned} \tag{9}$$

Therefore, (10) can be formulated using model analysis methods to obtain the exact solution for the parameters to be identified. However, in practical calculations, directly solving the high-order multivariate equation, as shown in (10), is difficult and requires significant computational resources. Hence, this article adopts the parameter identification method based on the optimization algorithms to avoid directly solving the high-order multivariable equation system, as shown in the following equation:

$$\begin{cases} Z(j\omega_1) = f(R_P, R_S, R_e, L_P, L_S, M, \omega_1) = \hat{Z}(j\omega_1) \\ Z(j\omega_2) = f(R_P, R_S, R_e, L_P, L_S, M, \omega_2) = \hat{Z}(j\omega_2) \\ \quad\quad\vdots \\ Z(j\omega_m) = f(R_P, R_S, R_e, L_P, L_S, M, \omega_m) = \hat{Z}(j\omega_m). \end{cases} \tag{10}$$

B. Establishment of Optimization Problem Models

To circumvent the solution of the high-order multivariate equations in (10), this article develops an objective function to convert the task of obtaining the exact solution for the high-order multivariate equations into a problem of verifying the suitability of the solution to mitigate the computational complexity.

The parameter vector to be identified, $\mathbf{P} = [R_P\ R_S\ R_e\ L_P\ L_S\ M]^{\mathrm{T}}$, is used to establish the objective function $F(\mathbf{P})$ as follows:

$$F(\mathbf{P}) = \frac{1}{m}\sum_{k=1}^{m}\left|Z(j\omega_k) - \hat{Z}(j\omega_k)\right|^2. \tag{11}$$

The objective function $F(\mathbf{P})$ is a function composed of the parameter vector to be identified. When the calculated value of the impedance $Z(j\omega_k)$ equals the measured value $\hat{Z}(j\omega_k)$, the objective function $F(\mathbf{P})$ attains its minimum value of 0. As shown in (12), the parameters R_P, R_S, R_e, L_P, L_S, and M, can be considered as the solution to (10).

Therefore, the problem of solving a high-order multivariate equation is transformed into an optimization problem of finding the minimum value of the objective function $F(\mathbf{P})$

$$\min_{R_P,\ldots,M} F(\mathbf{P}) = \min_{R_P,\ldots,M}\left[\frac{1}{m}\sum_{k=1}^{m}\left|Z(j\omega_k) - \hat{Z}(j\omega_k)\right|^2\right] = 0. \tag{12}$$

In practice, achieving exact convergence of the objective function $F(\mathbf{P})$ to the minimum value of 0 is difficult due to computational errors. Therefore, a small threshold value th needs to be set. When the objective function $F(\mathbf{P}) < \mathrm{th}$, it indicates that the convergence condition for $F(\mathbf{P})$ has been satisfied, as shown in the following equation:

$$\min_{R_P,\ldots,M} F(\mathbf{P}) = \min_{R_P,\ldots,M}\left[\frac{1}{m}\sum_{k=1}^{m}\left|Z(j\omega_k) - \hat{Z}(j\omega_k)\right|^2\right] < \mathrm{th}. \tag{13}$$

Furthermore, the parameters to be identified can be considered as the identified values of the system parameters based on (13).

C. GD Optimization Algorithm

The GD method is a commonly used method for solving optimization problems, offering better convergence, stability, and reliability compared with heuristic optimization algorithms.

Suppose the initial parameter vector is set as $\mathbf{P}^{(0)} = [R_P{}^{(0)}\ R_S{}^{(0)}\ R_e{}^{(0)}\ L_P{}^{(0)}\ L_S{}^{(0)}\ M^{(0)}]^{\mathrm{T}}$. After t iterations, the parameter vector becomes $\mathbf{P}^{(t)} = [R_P{}^{(t)}\ R_S{}^{(t)}\ R_e{}^{(t)}\ L_P{}^{(t)}\ L_S{}^{(t)}\ M^{(t)}]^{\mathrm{T}}$. The iteration formula for the GD method is given by

$$\mathbf{P}^{(t+1)} = \mathbf{P}^{(t)} - \boldsymbol{\alpha} \cdot \nabla F(\mathbf{P}^{(t)}) \tag{14}$$

where $\nabla F(\mathbf{P}^{(t)})$ represents the gradient of the objective function $F(\mathbf{P})$ at $\mathbf{P}^{(t)}$, and its expression is given by (15) and (16). α is the learning rate vector used to adjust the iteration step size

$$\nabla F = \left[\frac{\partial F}{\partial R_P}, \frac{\partial F}{\partial R_S}, \ldots, \frac{\partial F}{\partial M}\right]^{\mathrm{T}} = \left[\frac{\partial F}{\partial P_1}, \frac{\partial F}{\partial P_2}, \ldots, \frac{\partial F}{\partial P_n}\right]^{\mathrm{T}} \tag{15}$$

$$\frac{\partial F}{\partial P_i} = \frac{1}{m}\sum_{k=1}^{m}\begin{pmatrix} 2\left[R(j\omega_k) - \hat{R}(j\omega_k)\right] \times \frac{\partial R(j\omega_k)}{\partial P_i} \\ +2\left[X(j\omega_k) - \hat{X}(j\omega_k)\right] \times \frac{\partial X(j\omega_k)}{\partial P_i} \end{pmatrix}. \tag{16}$$

Assuming that the turns ratio between the transmitting coil and the receiving coil is 1: n. Based on (6), under the conditions

of the same coil material and shape, the ratio of R_S to R_P can be approximated by the turn ratio. Similarly, the ratio of L_S to R_P can also be approximated by the turns ratio, resulting in the approximate relationships $R_S = n{\cdot}R_P$ and $L_S = n{\cdot}L_P$.

D. Adam Optimization Algorithm

The traditional GD algorithm efficiently handles simple convex function optimization problems but often gets stuck in local optima when dealing with more complex nonconvex functions. The Adam optimization algorithm, an improvement over GD, is an adaptive learning rate method that introduces first- and second-moment estimates, combining the momentum and adaptive learning rate to handle more complex optimization problems.

The first-moment estimate introduces momentum, allowing the algorithm to escape local optimal solutions and achieve more accurate convergence. After t iterations, the first-moment estimate is denoted as $\mathbf{m}^{(t)}$ with the iteration formula

$$\mathbf{m}^{(t)} = \beta_1 \cdot \mathbf{m}^{(t-1)} + (1-\beta_1) \cdot \nabla F\left(\mathbf{P}^{(t)}\right) \tag{17}$$

where β_1 is a manually adjusted parameter that controls the effect of momentum.

The second-moment estimate adjusts the learning rate adaptively and brings different parameters to the same update level to identify more parameters accurately. After t iterations, the second-moment estimate is denoted as $\mathbf{v}(t)$ with the formula as follows:

$$\mathbf{v}^{(t)} = \beta_2 \cdot \mathbf{v}^{(t-1)} + (1-\beta_2) \cdot \left[\nabla F\left(\mathbf{P}^{(t)}\right)\right]^2. \tag{18}$$

Initially, both $\mathbf{m}^{(0)}$ and $\mathbf{v}^{(0)}$ are set to $\mathbf{0}$. To prevent interference, the Adam optimization algorithm corrects those estimates using those formulae

$$\tilde{\mathbf{m}}^{(t)} = \mathbf{m}^{(t)} / \left(1-\beta_1^t\right) \tag{19}$$

$$\tilde{\mathbf{v}}^{(t)} = \mathbf{v}^{(t)} / \left(1-\beta_2^t\right). \tag{20}$$

The parameter vector $\mathbf{P}$ is updated by

$$P_i^{(t+1)} = P_i^{(t)} - \frac{\alpha_i}{\sqrt{\tilde{v}_i^{(t)}} + \varepsilon} \cdot \tilde{m}^{(t)}, i = 1, 2, \ldots, k \tag{21}$$

where ε is a small value to prevent division by zero. Thus, the iterative formula for the Adam optimization algorithm is summarized as follows:

$$\begin{cases} \mathbf{m}^{(t)} = \beta_1 \cdot \mathbf{m}^{(t-1)} + (1-\beta_1) \cdot \nabla F(\mathbf{P}^{(t)}) \\ \mathbf{v}^{(t)} = \beta_2 \cdot \mathbf{v}^{(t-1)} + (1-\beta_2) \cdot \left[\nabla F(\mathbf{P}^{(t)})\right]^2 \\ \tilde{\mathbf{m}}^{(t)} = m^{(t)} / \left(1-\beta_1^t\right) \\ \tilde{\mathbf{v}}^{(t)} = v^{(t)} / \left(1-\beta_2^t\right) \\ P_i^{(t+1)} = P_i^{(t)} - \alpha_i \cdot \frac{\tilde{m}_i^{(t)}}{\sqrt{\tilde{v}_i^{(t)}} + \varepsilon}, i = 1, 2, \ldots, k. \end{cases} \tag{22}$$

E. Adam-W Optimization Algorithm

The objective function $F(\mathbf{P})$ in (11) accumulates the squared difference between the calculated impedance Z and the measured impedance $\hat{Z}$, which can be separated into its real and imaginary part, denoted as $\mathrm{Re}(F(\mathbf{P}))$ and $\mathrm{Im}(F(\mathbf{P}))$, respectively, as shown in the following equation:

$$\begin{cases} \mathrm{Re}(F(\mathbf{P})) = \frac{1}{m}\sum_{k=1}^{m}\left[R(j\omega_k) - \hat{R}(j\omega_k)\right]^2 \\ \mathrm{Im}(F(\mathbf{P})) = \frac{1}{m}\sum_{k=1}^{m}\left[X(j\omega_k) - \hat{X}(j\omega_k)\right]^2. \end{cases} \tag{23}$$

In the UWPT system, some parameters variation significantly impacts $\mathrm{Re}(F(\mathbf{P}))$, while others affect $\mathrm{Im}(F(\mathbf{P}))$. Understanding how different parameters influence the objective function $F(\mathbf{P})$ at different frequencies aids in parameter identification. However, traditional GD and Adam optimization algorithm maintain fixed and equal weights for $\mathrm{Re}(F(\mathbf{P}))$ and $\mathrm{Im}(F(\mathbf{P}))$ during iterations, causing coupling and hidden influences that affect identification accuracy.

To address this, we introduce weight parameters W for $\mathrm{Re}(F(\mathbf{P}))$ and Im $(F(\mathbf{P}))$, constructing a new weighted objective function $J(\mathbf{P})$

$$\begin{aligned} J(\mathbf{P}) &= W \cdot \mathrm{Re}(F(\mathbf{P})) + (1-W) \cdot \mathrm{Im}(F(\mathbf{P})) \\ &= \frac{1}{m}\sum_{k=1}^{m}\begin{pmatrix} W\left[R(j\omega_k) - \hat{R}(j\omega_k)\right]^2 \\ +(1-W)\left[X(j\omega_k) - \hat{X}(j\omega_k)\right]^2 \end{pmatrix}. \end{aligned} \tag{24}$$

By adjusting weights based on the influence characteristics of the parameters, the Adam-W algorithm reduces parameter coupling and improves multiparameter identification accuracy.

The gradient computation for $J(\mathbf{P})$ is given as follows:

$$\frac{\partial J}{\partial P_i} = \frac{1}{m}\sum_{k=1}^{m}\begin{pmatrix} 2W\left[R(j\omega_k) - \hat{R}(j\omega_k)\right]\frac{\partial R(j\omega_k)}{\partial P_i} \\ +2(1-W)\left[X(j\omega_k) - \hat{X}(j\omega_k)\right]\frac{\partial X(j\omega_k)}{\partial P_i} \end{pmatrix}. \tag{25}$$

The new convergence criterion is given as follows:

$$\min_{R_P, R_S, \ldots, M}\left\{\frac{1}{m}\sum_{k=1}^{m}\begin{pmatrix} W\left[R(j\omega_k) - \hat{R}(j\omega_k)\right]^2 \\ +(1-W)\left[X(j\omega_k) - \hat{X}(j\omega_k)\right]^2 \end{pmatrix}\right\} < \mathrm{th}. \tag{26}$$

The iterative update matrix of the Adam-W algorithm remains consistent with the Adam algorithm, as shown in (22). The parameter identification process based on the Adam-W algorithm for UWPT systems is illustrated in Fig. 4.

IV. Experimental Verification

To validate the effectiveness and accuracy of the proposed parameter identification method, a UWPT system experimental platform based on *SS* resonance compensation was established, as shown in Fig. 5. The platform includes a transmitting coil, receiving coil, resonance compensation, inverter, load resistor, dc power supply, and water tank. Both coils are wound with 30 turns of Litz wire with an inner diameter of 55 mm and an outer diameter of 150 mm. The water tank's salt concentration is 35‰, matching average seawater salinity.

Fig. 6 presents the circuit diagram of the UWPT system. Here, V_{dc} is the 24-V voltage supplied by the dc power source. The resonance compensation capacitors C_1 and C_2 have

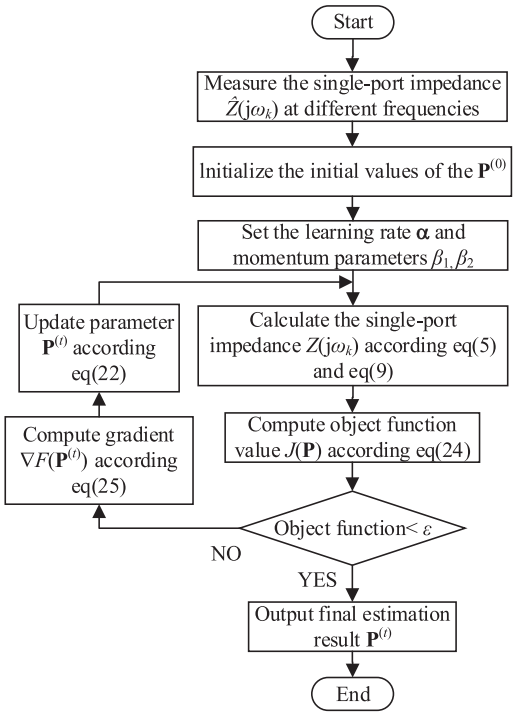

Fig. 4. Parameter identification process based on the Adam-W optimization algorithm.

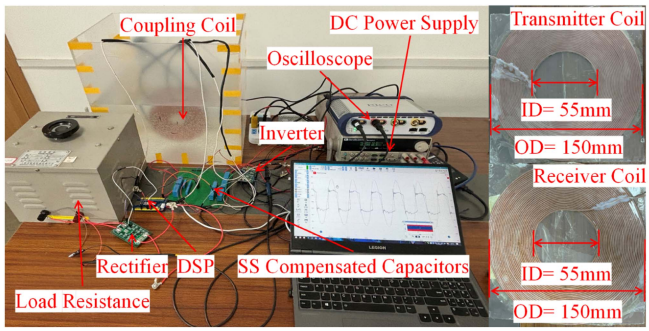

Fig. 5. UWPT system experimental platform.

capacitance values measured as 38.1 nF and 38.2 nF, respectively, and the load resistor R_A is 35 Ω. MOSFETs S_1–S_8 are BSC028N06NS, forming a full-bridge inverter (S_1–S_4) and a full-bridge rectifier (S_5–S_8). TMS320F28355 DSP from Texas Instruments is used and provides PWM signals for the inverter and rectifier.

Fig. 6 illustrates the flowchart for calculating the front-end port impedance $\hat{Z}$. Voltage v_p and current i_p are measured by the DSP and processed in MATLAB. They pass through a second-order bandpass filter to remove higher order harmonics, resulting in the fundamental voltage v_{p1} and current i_{p1}. The second-order bandpass filter is designed as follows:

$$H(s) = \frac{2\zeta\omega_0 s}{s^2 + 2\zeta\omega_0 s + \omega_0{}^2} \tag{27}$$

where the damping ratio ζ is 0.05.

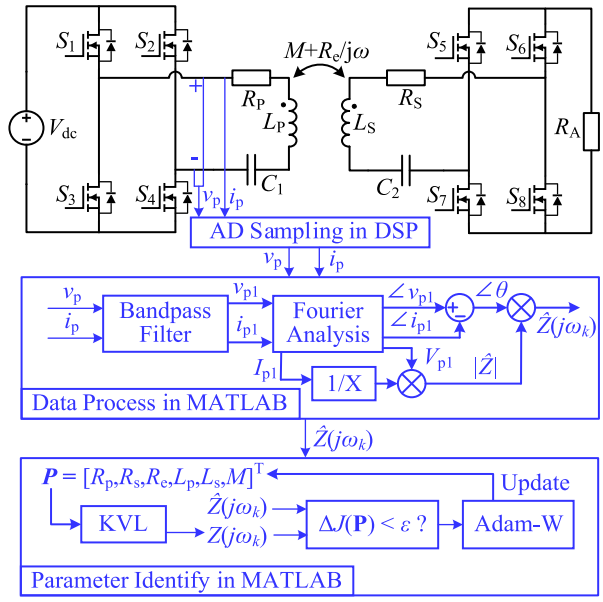

Fig. 6. Circuit schematic of the UWPT system.

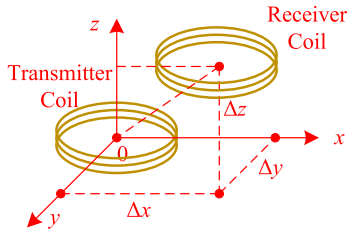

Fig. 7. Coil spatial distance diagram.

Fourier analysis of v_{p1} and i_{p1} provides the voltage amplitude V_{p1}, current amplitude I_{p1}, and phase difference θ. The magnitude $|\hat{Z}|$ of the front-end port impedance is obtained by dividing V_{p1} by I_{p1}, and calculated using Euler's formula, as shown in the following equation:

$$\begin{aligned}\hat{Z} &= (V_{p1}/I_{p1}) \times (\cos\theta + j\sin\theta) \\ &= \left|\hat{Z}\right| \times (\cos\theta + j\sin\theta) \\ &= \left|\hat{Z}\right| e^{j\theta}.\end{aligned} \tag{28}$$

A. Parameter Identification of UWPT System

When the transmitting coil is aligned with the receiving coil with no horizontal offset ($\Delta x = \Delta y = 0$ cm) and a coil separation distance of $\Delta z = 3$ cm, as shown in Fig. 7, the UWPT system operates at 75 kHz. We use four different optimization algorithms—PSO, traditional GD, Adam, and Adam-W—to identify the equivalent parameters of the coupler online.

According to (6), the parameters of the UWPT system's coupler change with frequency due to the eddy current effect. To minimize frequency variation impact, four sets of frequencies around the operating frequency of 75 kHz were selected as sampling frequencies. Different input voltages v_p and input currents i_p are measured at those frequencies, and their fundamental

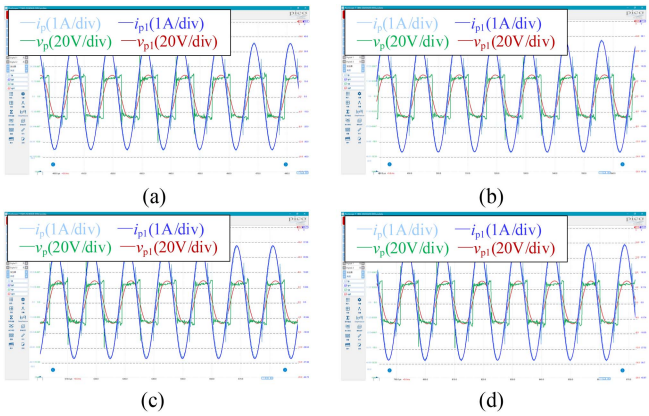

Fig. 8. Measured input voltage v_p and current i_p, and the fundamental components v_{p1} and i_{p1} at different frequencies: (a) 74.500 kHz; (b) 74.800 kHz; (c) 75.200 kHz; (d) 75.500 kHz.

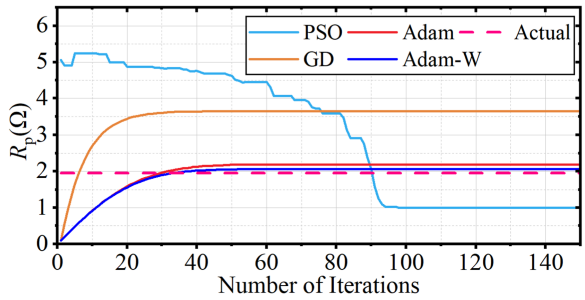

Fig. 9. R_p iteration process diagram for four algorithms.

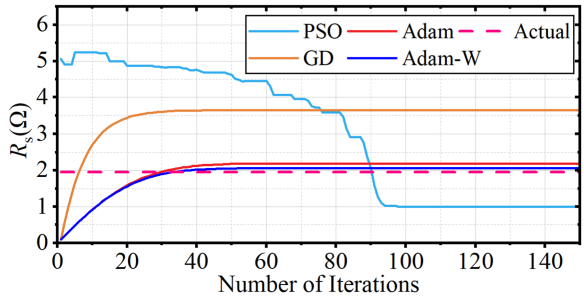

Fig. 10. R_s iteration process diagram for four algorithms.

TABLE I
MEASURED FRONT-END PORT IMPEDANCE $\hat{Z}$

f/kHz	Re($\hat{Z}$)/Ω	Im($\hat{Z}$) /Ω
74.500	5.5714	–3.9146
74.800	5.6077	–3.4833
75.200	5.6425	–3.0552
75.500	5.6510	–2.9486

components v_{p1} and i_{p1} were obtained by filtering out higher order harmonics, as shown in Fig. 8.

Based on those fundamental components, the measured front-end port impedance $\hat{Z}(j\omega)$ for four frequencies near 75 kHz is shown in Table I. The initial set values of the parameter vector $\mathbf{P}^{(0)}$ for identification are shown in Table II. The learning rate

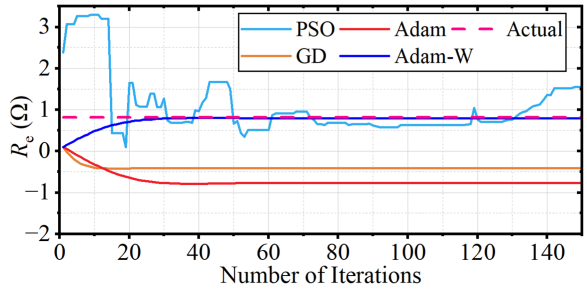

Fig. 11. R_e iteration process diagram for four algorithms.

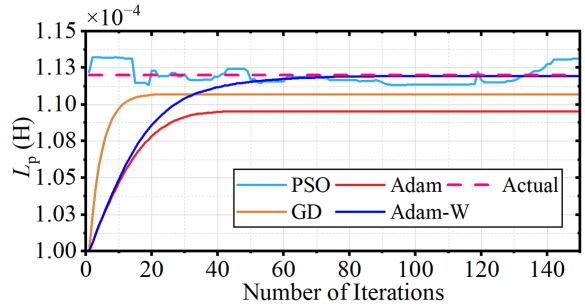

Fig. 12. L_p iteration process diagram for four algorithms.

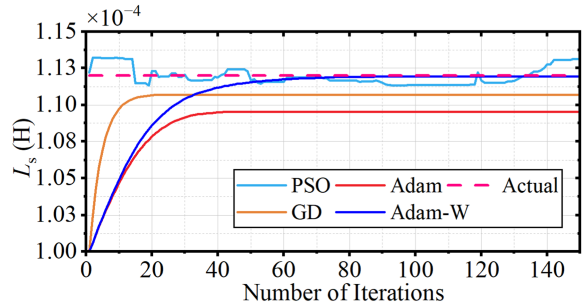

Fig. 13. L_s iteration process diagram for four algorithms.

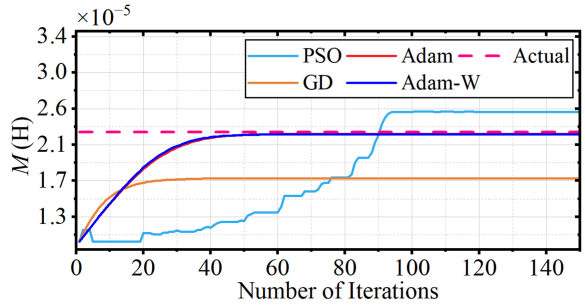

Fig. 14. M iteration process diagram for four algorithms.

TABLE II
INITIAL PARAMETER VALUES FOR IDENTIFICATION

Parameter	R_P	R_S	R_e	L_P	L_S	M
Value	0.10 Ω	0.10 Ω	0.10 Ω	100 μH	100 μH	10.0 μH

TABLE III
IDENTIFICATION RESULTS OF FOUR KINDS OF ALGORITHMS

Parameter		R_p, R_s/Ω	R_e/Ω	L_P, L_s/μH	M/μH	Conv.
Meas.		1.95	0.82	112.0	23.1	
PSO	Ident.	1.00	2.23	114.5	25.6	150
	Error	48.7%	244%	0.63%	10.0%	
PSO	Ident.	1.9498	0.8206	112.0	23.102	10000
	Error	0.10‰	0.73‰	0.00‰	0.09‰	
GD	Ident.	3.65	-0.40	110.7	16.0	45
	Error	87.0%	149%	1.16%	24.2%	
Adam	Ident.	2.19	-0.76	109.5	21.7	62
	Error	12.3%	192%	2.23%	6.06%	
Adam-W	Ident.	2.02	0.79	111.95	22.7	95
	Error	3.6%	3.6%	0.045%	1.73%	

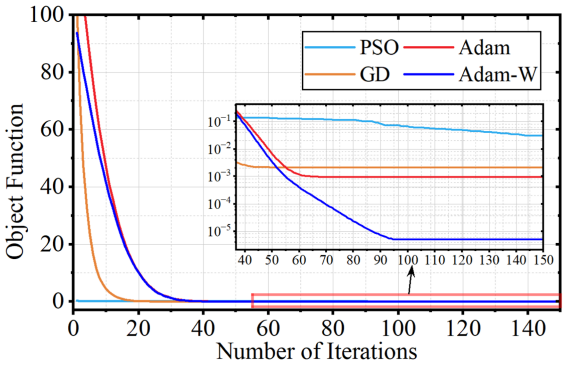

Fig. 15. Convergence process of objective functions.

vector α for the GD algorithm is set to $[10^{-1}, 10^{-1}, 10^{-1}, 10^{-12}, 10^{-12}, 10^{-12}]^T$, β_1 and β_2 for the Adam algorithm are set to 0.1 and 0.99. W for Adam-W algorithm is set to 0.99, and the number of particles in the swarm POP of PSO algorithm is set to 300.

The PSO algorithm iterates by updating the global best within the population; convergence cannot be determined using the condition $\Delta F(\mathbf{P}) < \varepsilon$. Therefore, 150 iterations and 10 000 iterations are selected for comparison with traditional GD, Adam, and Adam-W algorithms. The identification results are shown in Table III, and the processes of identification are shown in Figs. 9–14.

Overall, L_P and L_S showed the best identification results, followed by M. R_e, R_S, and R_P had relatively large errors. The traditional GD algorithm has the highest average error at 58.25%, while the Adam algorithm had 37.85%. The Adam-W algorithm effectively improved accuracy, reducing the average by 2.103%. Unlike GD-based algorithms, the iteration curves indicate that the PSO algorithm exhibits nonlinear characteristics due to its incorporation of stochastic factors. At 150 iterations, the average identification error of the PSO algorithm is 58.77%. The PSO, GD, Adam, and Adam-W algorithms approximately take 0.5 s, 0.6 s, 1.0 s, and 1.5 s, respectively. At 10 000 iterations, the average identification error of the PSO algorithm is minimal at 0.17‰, but it requires a significantly long computation time, approximately 75 s.

The iterative processes of the objective functions for four algorithms are shown in Fig. 15. The PSO algorithm converges to a value of 3.072×10^{-2} for the objective function after 150 iterations. The GD algorithm stabilized after 40 iterations with a result of 2.07×10^{-3}. The Adam algorithm converged after 65 iterations (1.6 × longer than GD) with a result of 9.47×10^{-4}. The Adam-W algorithm, which adds weighted parameters to the objective function, converged after 95 iterations (2.4 × longer than GD) with the smallest result of 4.05×10^{-6}.

TABLE IV
SENSITIVITY ANALYSIS OF THE PARAMETERS TO BE IDENTIFIED

	REAL	IMAG
$0.1\times\partial Z/\partial R_P(\Omega/\Omega)$	0.1	0
$0.1\times\partial Z/\partial R_S(\Omega/\Omega)$	0.1	0
$0.1\times\partial Z/\partial R_e(\Omega/\Omega)$	1.3632×10^{-3}	-6.7716×10^{-2}
$\partial Z/\partial L_P(\Omega/\mu H)$	0	4.7124×10^{-1}
$\partial Z/\partial L_S(\Omega/\mu H)$	0	4.7124×10^{-1}
$\partial Z/\partial M(\Omega/\mu H)$	3.1910×10^{-1}	6.4240×10^{-3}

B. Parameter Sensitivity Analysis

The objective function, as indicated by (11) and (24), is composed of the sum of squares of the error between the measured impedance value $\hat{Z}$ at the front-end port of the UWPT system and the calculated impedance value Z obtained through the identification parameters. The purpose of this method is to identify how different parameters affect the front-end port impedance Z at different angular frequencies ω. Sensitivity analysis is performed on the front-end port impedance Z using the experimental data of the UWPT system. The ranges of variation for the parameters R_P and R_S are between 0.1 and 1.9 Ω, and for R_e between 0.1 and 0.82 Ω. Given that the change amplitude per iteration is much smaller than 1 Ω, error corrections are applied to R_P, R_S, and R_e. The sensitivity analysis results after correction are shown in Table IV.

From the sensitivity analysis in Table IV, it can be observed that the variation in M has the greatest impact on the real part of the front-end port impedance value Z, while L_P and L_S have the greatest impact on the imaginary part of the front-end port impedance value Z. Therefore, the identification errors for L_P, L_S, and M are relatively small when using the three algorithms. Conversely, R_P, R_S, and R_e have a smaller impact on Z, resulting in larger identification errors when using three algorithms. The variation in R_e has a relatively small impact on both the real and imaginary parts of Z, leading to the largest identification relation error. This sensitivity analysis provides crucial insights into why certain parameters exhibit larger identification errors and helps guide future improvements in the parameter identification process.

C. Analysis of Weight Parameters in Adam-W Algorithm

Fig. 16 shows the variation of the real and imaginary parts of the objective function during the descent process of the Adam and Adam-W optimization algorithm.

From Fig. 16(a), it is evident that, at the beginning of the iteration process, $\mathrm{Re}(F(\mathbf{P}))$ and $\mathrm{Im}(F(\mathbf{P}))$ have similar proportional weights. According to Table IV, R_e impacts both the real and imaginary parts of the objective function. However, the negative

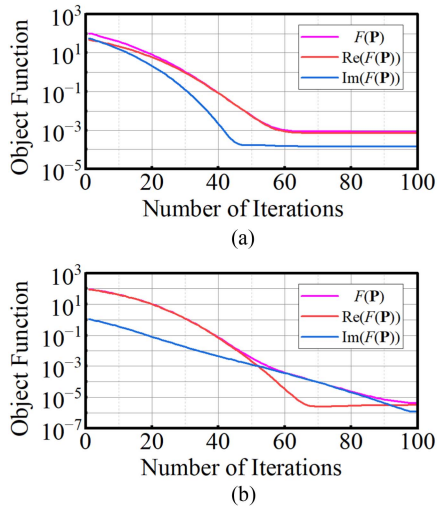

Fig. 16. Comparison of the descent of the objective function under Adam and Adam-W optimization algorithms. (a) Adam optimization algorithm. (b) Adam-W optimization algorithm.

sensitivity of the imaginary part and the lower sensitivity of the real part conceal the characteristic information of R_e, leading to an initial iteration direction error. The Adam-W algorithm addresses this by setting the weight parameter W to 0.99, which separates the real part Re(J(**P**)) and the imaginary part Im(J(**P**)) of the objective function. This adjustment makes the real part approximately 100 × larger than the imaginary part, enhancing its influence during the iteration process.

By adjusting the weight parameter W to separate the real and imaginary parts of the objective function, the Adam-W algorithm effectively handles multiparameter identification problems, leveraging the specific characteristics of each parameter in the identification model.

D. Parameter Identification of UWPT System Under Coupling Coils Misalignment

To analyze coil misalignment caused by submarine wave, the spatial distance between the transmission coils and the receiving coils of the UWPT system is varied, as shown in Fig. 7. The PSO, traditional GD, Adam, and Adam-W algorithms are used to identify the coupler parameters.

With a spacing of $\Delta z = 3$ cm, a lateral offset of $\Delta x = 1$ cm, and no vertical offset of $\Delta y = 0$ cm, the identification results of the equivalent parameters using the PSO, traditional GD, Adam, and Adam-W algorithms are shown in Table V. The average error for the GD is 56.29%, for the Adam is 43.7%, and for the Adam-W is 3.91%, and for PSO is 36.5% at 150 iterations and for PSO is 1.1‰ at 10 000 iterations.

With a spacing of $\Delta z = 3$ cm, a vertical offset of $\Delta y = 1$ cm, and no lateral offset of $\Delta x = 0$ cm, the identification results are shown in Table VI. The average error for the GD is 53.03%, for the Adam is 39.52%, and for the Adam-W algorithm is 2.4%, and for PSO is 16.29% at 150 iterations and for PSO is 0.42‰ at 10 000 iterations.

TABLE V
IDENTIFICATION RESULTS WHEN $\Delta X = 1$ CM, $\Delta Y = 0$ CM, AND $\Delta Z = 3$ CM

Parameter		R_p, R_s/Ω	R_e/Ω	L_P, L_s/μH	M/μH	Conv.
Meas.		1.70	0.7	113.2	20.1	
PSO	Ident.	1.33	1.86	114.9	21.4	150
	Error	21.8%	166%	1.5%	6.47%	
PSO	Ident.	1.6992	0.70038	113.2	20.103	10000
	Error	0.47‰	5.4‰	0.0‰	0.15‰	
GD	Ident.	2.86	−0.55	111.9	16.0	42
	Error	68%	179%	1.14%	20.5%	
Adam	Ident.	1.74	−1.06	110.7	20.5	61
	Error	2.4%	251%	2.2%	2.0%	
Adam-W	Ident.	1.82	0.65	113.1	19.7	94
	Error	7.1%	7.1%	0.09%	2.0%	

TABLE VI
IDENTIFICATION RESULTS WHEN $\Delta X = 0$ CM, $\Delta Y = 1$ CM, AND $\Delta Z = 3$ CM

Parameter		R_p, R_s/Ω	R_e/Ω	L_p,L_s/μH	M/μH	Conv.
Meas.		1.80	0.82	113.0	20.3	
PSO	Ident.	1.87	0.1	112.6	20.0	150
	Error	3.9%	87.8%	0.35%	1.48%	
PSO	Ident.	1.799	0.819	113.0	20.303	10000
	Error	0.56‰	1.22‰	0.0‰	0.15‰	
GD	Ident.	2.97	−0.51	111.6	16.1	44
	Error	65%	162%	1.24%	20.7%	
Adam	Ident.	1.81	−1.01	110.4	20.8	65
	Error	0.55%	223%	2.30%	2.46%	
Adam-W	Ident.	1.88	0.81	112.8	20.0	92
	Error	4.4%	1.21%	0.18%	1.48%	

TABLE VII
IDENTIFICATION RESULTS WHEN $\Delta X = 0$ CM, $\Delta Y = 0$ CM, AND $\Delta Z = 4$ CM

Parameter		R_p, R_s/Ω	R_e/Ω	L_P, L_s/μH	M/μH	Conv.
Meas.		1.65	0.65	117.0	17.5	
PSO	Ident.	2.06	2.43	118.9	16.7	150
	Error	24.8%	274%	1.62%	4.57%	
PSO	Ident.	1.6497	0.6508	117.0	17.501	10000
	Error	0.18‰	1.23‰	0.0‰	0.06‰	
GD	Ident.	2.26	−0.86	115.4	15.1	43
	Error	87.0%	232%	1.16%	24.2%	
Adam	Ident.	1.06	−1.09	114.1	20.0	64
	Error	35.8%	267%	2.48%	14.3%	
Adam-W	Ident.	1.54	0.69	116.6	17.9	92
	Error	6.7%	6.15%	0.51%	2.23%	

With a spacing of $\Delta z = 4$ cm, no lateral offset ($\Delta x = 0$ cm), and no vertical offset ($\Delta y = 0$ cm), the identification results are shown in Table VII. The average error for the GD is 72.08%, for the Adam algorithm is 59.64%, and for the Adam-W is 3.8%, and for PSO is 55.24% at 150 iterations and for PSO is 0.275‰ at 10 000 iterations.

E. Parameter Identification of UWPT System Under High-Salinity Seawater Environment

The salinity of seawater varies due to factors, such as the latitude of the sea area, climate, and seasonal changes. Consequently, the eddy current effects produced by the seawater's electrical conductivity also change. Therefore, this article conducts parameter identification for the UWPT system in a high-salinity seawater environment (50‰) with four different algorithms, and the result is shown in Table VIII. The average error for the GD is

TABLE VIII
IDENTIFICATION RESULTS IN HIGH-SALINITY SEAWATER ENVIRONMENT

Parameter		R_p, R_s/Ω	R_e/Ω	L_P, L_s/μH	M/μH	Conv.
Meas.		2.1	0.97	110.0	21.0	
PSO	Ident.	2.38	0.1	108.8	20.3	150
	Error	13.3%	89.7%	1.09%	3.33%	
PSO	Ident.	2.1003	0.9714	110.0	21.001	10000
	Error	0.14‰	1.44‰	0.0‰	0.05‰	
GD	Ident.	3.3	–0.26	108.8	16.6	48
	Error	57.1%	127%	1.09%	20.9%	
Adam	Ident.	2.05	–0.48	107.9	21.6	67
	Error	2.4%	149%	1.9%	2.9%	
Adam-W	Ident.	2.04	0.94	109.9	21.2	98
	Error	2.9%	3.1%	0.09%	0.95%	

TABLE IX
COMPARISON BETWEEN THE EXISTING RELATED RESEARCH WORKS

Ref.	Num. of parameters	error	Iterations	Additional conditions
[20]	2	<1%	1	Coupler mutual
[21]	2	<1%	1	Coupler mutual
[22]	2	<2%	1	Current sensor
[27]	2	<3%	1	Training dataset
[29]	7	<10%	<1000	No
[30]	4–8	<10%	<3500	No
This work	6	<4%	<100	No

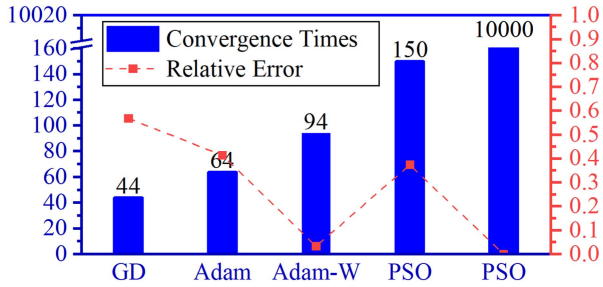

Fig. 17. Comparison of convergence iterations and relative errors for three algorithms.

44.05%, for the Adam algorithm is 26.75%, and for the Adam-W is 1.67%, and for PSO is 20.3% at 150 iterations and for PSO is 0.295‰ at 10 000 iterations.

F. Results of Parameter Identification Experiments

In the UWPT system established in this study, the parameters L_p and L_s exhibit the highest sensitivity to the imaginary part of the impedance $Z(j\omega)$, resulting in the highest identification accuracy. The parameter M shows the greatest sensitivity to the real part of the impedance $Z(j\omega)$, with slightly lower identification accuracy. The identification accuracy for R_p and R_s is next, followed by the parameter R_e, which has the lowest sensitivity to both the real and imaginary parts of the impedance $Z(j\omega)$, resulting in the largest identification error.

The comprehensive average identification error of the GD algorithm is 56.74%, with an iteration count of 44 and an identification time of approximately 0.5 s. The Adam algorithm, compared with the GD algorithm, introduces the first-order moment estimation to escape local optima and second-order moment estimation to enhance multiparameter identification capability, thereby further improving parameter identification accuracy to 41.49%. However, this comes at the cost of an increased iteration count of 64 and an identification time of approximately 0.6 s. By incorporating weight parameters, the Adam-W algorithm effectively improves the accuracy of multiparameter identification by adjusting the structure of the objective function. The average identification error is approximately 2.78%, with an increased iteration count of 94 and an identification time of around 1.0 s. The PSO algorithm, within 150 iterations, shows a relatively large identification error, averaging 37.42%, and exhibits nonlinear variations with some randomness during the identification process. However, after 10 000 iterations, the PSO algorithm demonstrates its global search advantage, achieving a very small identification error of approximately 0.452‰, but requires a significantly long computation time of around 75 s, as shown in Fig. 17.

Considering all factors, the Adam-W algorithm proposed in this study offers higher computational accuracy within a relatively short time, making it more adaptable to the challenging underwater environments characterized by submarine wave.

G. Comparison of Existing Methods

Existing parameter monitoring methods mainly fall into three categories: analytical model methods, data-driven methods, and system model methods. Analytical model methods, as demonstrated in [20], [21], and [22], offer fast identification speed and small identification errors, but typically identify few parameters and require additional hardware, making them unsuitable for complex systems. Data-driven methods, as shown in [27], are relatively fast but require pretraining datasets, posing engineering challenges. System model methods combine the advantages of both by transforming the identification problem into an optimization problem, thereby significantly reducing computational complexity and enabling the identification of more parameters. Jiang et al. [29] utilized a genetic algorithm to identify seven characteristic parameters of a dc/dc converter. Yang et al. [30] employed a dual-layer evolutionary algorithm to identify 4–8 parameters of a WPT system. However, these heuristic optimization algorithms are inherently stochastic and may lead to poor stability and reliability of the identification results, as well as longer identification times due to the high number of iterations. This study employs GD-type algorithms, known for their good convergence stability and faster convergence compared with heuristic optimization algorithms. Experimental results demonstrate that this method achieves an average identification error of less than 4% for the six characteristic parameters of UWPT coupler, with fewer than 100 iterations and significantly fewer than heuristic optimization algorithms. The comparison of related work in the field of WPT system parameter identification is shown in Table IX.

V. Conclusion

This article proposes a parameter identification method based on the Adam-W optimization algorithm to address the complex multiparameter identification problem in UWPT systems. Unlike the traditional analytical methods that solve circuit matrix equations or transfer functions, this method converts the problem into an optimization problem, significantly reducing computational demands. This method requires only the detection of the input current and voltage, enabling the online monitoring of multiple characteristic parameters of the system's coupler without additional hardware.

The identification model established in this article can incorporate various parameter changes in real marine conditions, including seawater eddy effects, variations in seawater salinity, seawater pressure-magnetic effects, and misalignment of underwater coils. Four optimization algorithms—PSO, traditional GD, Adam, and Adam-W—were employed to perform online identification of six coupler parameters of UWPT system to verify the effectiveness of the proposed method. The experimental results show that the PSO algorithm in 10 000 iterations exhibits an extreme low identification error of 0.452‰ requiring a lengthy identification time of 75 s. In contrast, the Adam-W algorithm achieves good parameter identification accuracy within 1 s, with an average error of 2.78%, which is lower than 56.74% achieved by GD, 41.49% by Adam, and 37.42% by PSO in 150 iterations. Therefore, the Adam-W algorithm achieves higher accuracy in parameter identification of the UWPT system within a shorter time and demonstrates better applicability in seawater environments.

Future research may focus on improving the speed and accuracy of online parameter identification by combining analytical model methods to process parameters with different characteristics in batches and establish an experimental platform in real ocean environments to validate the effectiveness of the proposed method and further improve it based on the actual conditions.

References

[1] J. Li, G. Zhang, C. Jiang, and W. Zhang, "A survey of maritime unmanned search system: Theory, applications and future directions," *Ocean Eng.*, vol. 285, Oct. 2023, Art. no. 115359.

[2] F. Liu et al., "Review on fault-tolerant control of unmanned underwater vehicles," *Ocean Eng.*, vol. 285, Oct. 2023, Art. no. 115471.

[3] Y. R. Petillot, G. Antonelli, G. Casalino, and F. Ferreira, "Underwater robots: From remotely operated vehicles to intervention-autonomous underwater vehicles," *IEEE Robot. Automat. Mag.*, vol. 26, no. 2, pp. 94–101, Jun. 2019.

[4] A. Sahoo, S. K. Dwivedy, and P. S. Robi, "Advancements in the field of autonomous underwater vehicle," *Ocean Eng.*, vol. 181, pp. 145–160, Jun. 2019.

[5] Q. Han, H. Chen, W. Yang, Y. Zhang, J. Yang, and Y. Chen, "Analysis of reciprocating O-ring seal in the pressure-balanced oil-filled wet-mate electrical connectors for underwater applications," *Lubrication Sci.*, vol. 31, no. 7, pp. 335–345, 2019.

[6] M. Tefferi, M. Ghassemi, C. Calebrese, Q. Chen, and Y. Cao, "Characterizations of solid-liquid interface in a wet-mate subsea HVDC connector," *J. Electrostatic*, vol. 94, pp. 51–59, Aug. 2018.

[7] C. Cai, S. Wu, Z. Zhang, L. Jiang, and S. Yang, "Development of a fit-to-surface and lightweight magnetic coupler for autonomous underwater vehicle wireless charging systems," *IEEE Trans. Power Electron.*, vol. 36, no. 9, pp. 9927–9940, Sep. 2021.

[8] C. R. Teeneti, T. T. Truscott, D. N. Beal, and Z. Pantic, "Review of wireless charging systems for autonomous underwater vehicles," *IEEE J. Ocean. Eng.*, vol. 46, no. 1, pp. 68–87, Jan. 2021.

[9] D. Wang, F. Chen, J. Zhang, S. Cui, Z. Bie, and C. Zhu, "A novel pendulum-type magnetic coupler with high misalignment tolerance for AUV underwater wireless power transfer systems," *IEEE Trans. Power Electron.*, vol. 38, no. 12, pp. 14861–14871, Dec. 2023.

[10] Z. Zhang, H. Pang, A. Georgiadis, and C. Cecati, "Wireless power transfer—An overview," *IEEE Trans. Ind. Electron.*, vol. 66, no. 2, pp. 1044–1058, Feb. 2019.

[11] Z. Bi, T. Kan, C. C. Mi, Y. Zhang, Z. Zhao, and G. A. Keoleian, "A review of wireless power transfer for electric vehicles: Prospects to enhance sustainable mobility," *Appl. Energy*, vol. 179, pp. 413–425, Oct. 2016.

[12] X. Kang, C. Xiyou, and L. Danning, "Electrical impedance transformation techniques for an ultrasonic coupling wireless power transfer system under sea water," *Proc. Chin. Soc. Elect. Eng.*, vol. 35, no. 17, pp. 4461–4467, Sep. 2015.

[13] H. Zhang and F. Lu, "Insulated coupler structure design for the long-distance freshwater capacitive power transfer," *IEEE Trans. Ind. Inform.*, vol. 16, no. 8, pp. 5191–5201, Aug. 2020.

[14] D. Wang, J. Zhang, S. Cui, Z. Bie, F. Chen, and C. Zhu, "The state-of-the-arts of underwater wireless power transfer: A comprehensive review and new perspectives," *Renewable Sustain. Energy Rev.*, vol. 189, Jan. 2024, Art. no. 113910.

[15] K. Zhang, Y. Ma, Z. Yan, Z. Di, B. Song, and A. P. Hu, "Eddy current loss and detuning effect of seawater on wireless power transfer," *IEEE J. Emerg. Sel. Topics Power Electron.*, vol. 8, no. 1, pp. 909–917, Mar. 2020.

[16] P. Sun et al., "Eddy current loss analysis and frequency optimization design of double-sided LCC-IPT system in seawater environment," *Sci. China Technol. Sci.*, vol. 65, no. 2, pp. 407–418, Feb. 2022.

[17] T. Orekan, P. Zhang, and C. Shih, "Analysis, design, and maximum power-efficiency tracking for undersea wireless power transfer," *IEEE J. Emerg. Sel. Topics Power Electron.*, vol. 6, no. 2, pp. 843–854, Jun. 2018.

[18] Y.-G. Su, L. Chen, X.-Y. Wu, A. P. Hu, C.-S. Tang, and X. Dai, "Load and mutual inductance identification from the primary side of inductive power transfer system with parallel-tuned secondary power pickup," *IEEE Trans. Power Electron.*, vol. 33, no. 11, pp. 9952–9962, Nov. 2018.

[19] Y. Guo, Y. Zhang, W. Zhang, and L. Wang, "Battery parameter identification based on wireless power transfer system with rectifier load," *IEEE Trans. Ind. Electron.*, vol. 68, no. 8, pp. 6893–6904, Aug. 2021.

[20] J. Yin, D. Lin, C.-K. Lee, and S. Y. R. Hui, "A systematic approach for load monitoring and power control in wireless power transfer systems without any direct output measurement," *IEEE Trans. Power Electron.*, vol. 30, no. 3, pp. 1657–1667, Mar. 2015.

[21] J. Yin, D. Lin, C. K. Lee, T. Parisini, and S. Y. Hui, "Front-end monitoring of multiple loads in wireless power transfer systems without wireless communication systems," *IEEE Trans. Power Electron.*, vol. 31, no. 3, pp. 2510–2517, Mar. 2016.

[22] J. Zeng, Y. Yang, K. Li, S. Chen, and S. Y. R. Hui, "An ultrafast estimation method for coupling coefficient and receiver resonant frequency in universal wireless power transfer systems," *IEEE Trans. Power Electron.*, vol. 39, no. 4, pp. 4870–4883, Apr. 2024.

[23] X. Dai, X. Li, Y. Li, and A. P. Hu, "Maximum efficiency tracking for wireless power transfer systems with dynamic coupling coefficient estimation," *IEEE Trans. Power Electron.*, vol. 33, no. 6, pp. 5005–5015, Jun. 2018.

[24] Y. Liu and H. Feng, "Maximum efficiency tracking control method for WPT system based on dynamic coupling coefficient identification and impedance matching network," *IEEE J. Emerg. Sel. Topics Power Electron.*, vol. 8, no. 4, pp. 3633–3643, Dec. 2020.

[25] D.-H. Kim, S. Kim, S.-W. Kim, J. Moon, I. Cho, and D. Ahn, "Coupling extraction and maximum efficiency tracking for multiple concurrent transmitters in dynamic wireless charging," *IEEE Trans. Power Electron.*, vol. 35, no. 8, pp. 7853–7862, Aug. 2020.

[26] S. Mohagheghi, R. G. Harley, T. G. Habetler, and D. Divan, "Condition monitoring of power electronic circuits using artificial neural networks," *IEEE Trans. Power Electron.*, vol. 24, no. 10, pp. 2363–2367, Oct. 2009.

[27] Y. Su, J. Yang, X. Dai, J. Liu, and X. Hou, "TensorFlow neural network based load and mutual inductance identification method for magnetic coupling resonant wireless power transfer system," *Autom. Electr. Power Syst.*, vol. 45, no. 18, pp. 162–169, Sep. 2021.

[28] S. Zhao, F. Blaabjerg, and H. Wang, "An overview of artificial intelligence applications for power electronics," *IEEE Trans. Power Electron.*, vol. 36, no. 4, pp. 4633–4658, Apr. 2021.

[29] Y. Jiang, Y. Yu, and X. Peng, "Online anomaly detection in DC/DC converters by statistical feature estimation using GPR and GA," *IEEE Trans. Power Electron.*, vol. 35, no. 10, pp. 10945–10957, Oct. 2020.

[30] Y. Yang, S.-C. Tan, and S. Y. R. Hui, "Front-end parameter monitoring method based on two-layer adaptive differential evolution for SS-compensated wireless power transfer systems," *IEEE Trans. Ind. Inform.*, vol. 15, no. 11, pp. 6101–6113, Nov. 2019.
[31] J. Nayak, H. Swapnarekha, B. Naik, G. Dhiman, and S. Vimal, "25 years of particle swarm optimization: Flourishing voyage of two decades," *Arch. Comput. Methods Eng.*, vol. 30, no. 3, pp. 1663–1725, Apr. 2023.
[32] R. Bassily, V. Feldman, C. Guzmán, and K. Talwar, "Stability of stochastic gradient descent on nonsmooth convex losses," *Proc. NeurIPS*, vol. 33, pp. 4381–4391, Dec. 2020.
[33] K. Yuan, Q. Ling, and W. Yin, "On the convergence of decentralized gradient descent," *SIAM J. Optim.*, vol. 26, no. 3, pp. 1835–1854, 2016.
[34] D. P. Kingma and J. Ba, "Adam: A method for stochastic optimization," in *Proc. 3rd Int. Conf. Learn. Representation*, 2015, pp. 1–15.
[35] Y. Zhengchao et al., "Review on inductive wireless power transfer technology for underwater vehicles," *Proc. Chin. Soc. Elect. Eng.*, vol. 43, no. 24, pp. 9668–9681, Nov. 2023.

Bo Luo (Senior Member, IEEE) received the B.Sc. degree in electrical engineering and automation and the Ph.D. degree in electrical engineering from Southwest Jiaotong University, Chengdu, China, in 2014 and 2021, respectively.

From 2018 to 2019, he was a joint Ph.D. student with the University of Auckland, Auckland, New Zealand. He was a Postdoctoral Researcher with the City University of Hong Kong, Hong Kong, from 2022 to 2023. He is currently an Associate Professor with Yantai Research Institute, Harbin Engineering University, Harbin, China. His research focuses on high-frequency converters and circuits.

Huan Wu received the B.S. degree in measurement and control technology and instrument from Northeastern University, Shenyang, China, in 2021. He is currently working toward the Ph.D. degree in control science and engineering with Yantai Research Institute, Harbin Engineering University, Harbin, China.

His research focuses on wireless power transfer.

Mengyao Wang received the B.Sc. degree in communications engineering from Jilin University, Changchun, China, in 2023. She is currently working toward the M.Sc. degree in electronic and information engineering with Harbin Engineering University, Harbin, China.

Her major research direction is undersea wireless power transfer and simultaneous wireless power and data transfer.

Fangrui Wang received the B.Sc. degree in smart grid information engineering from the Qingdao University of Science and Technology, Qingdao, China, in 2014, and the M.Sc. degree in electrical engineering in 2021 from Harbin Engineering University, Harbin, China, where he is currently working toward the Doctorate degree in control science and is engaging in research on inductively coupled power transfer.

Longlei Bai received the B.S. and Ph.D. degrees in electrical engineering from Southwest Jiaotong University, Chengdu, China, in 2014 and 2020, respectively.

He is currently a Lecturer with Yantai Research Institute and the College of Intelligent Systems Science and Engineering, Harbin Engineering University, Harbin, China. His research interests include the design of wireless power transfer system and novel measurement method for power cable condition.

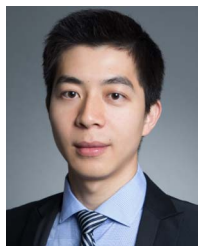

Chaoqiang Jiang (Senior Member, IEEE) received the B.Eng. and M.Eng. (First Class Honors) degrees in electrical engineering and automation from Wuhan University, Wuhan, China, in 2012 and 2015, respectively, and the Ph.D. degree in electrical and electronic engineering from The University of Hong Kong, Hong Kong, in 2019.

He is currently an Assistant Professor with the Department of Electrical Engineering and a faculty member with the State Key Laboratory of Terahertz and Millimeter Waves, City University of Hong Kong, Hong Kong. From 2019 to 2021, he was a Postdoctoral Research Associate with the University of Cambridge, Cambridge, U.K., where he has been affiliated with Clare Hall since 2021. In 2019, he was a Visiting Researcher with Nanyang Technological University, Singapore. His research interests include power electronics, wireless power transfer, electric machines and drives, and electric vehicle technologies.

Dr. Jiang was the recipient of CENG Research Excellence Award, Gold Medal at the Silicon Valley International Invention Festival, Gold Medals with Congratulations of the Jury in International Exhibition of Inventions of Geneva, Winner of CAPE Acorn Blue Sky Research Award at the University of Cambridge, Gold Medal in 3rd Asia Exhibition of Innovations and Inventions, Silver Award and Bronze Award in Shenzhen Qianhai Youth Innovation and Entrepreneurship Competition, and First Prize in the Interdisciplinary Research Competition at the University of Hong Kong. He is currently an Associate Editor for *IET Renewable Power Generation* and a Guest Editor for the *IEEE Open Journal of Vehicular Technology* and IEEE TRANSACTIONS ON POWER ELECTRONICS LETTERS.

Jiang You (Member, IEEE) received the Ph.D. degree in control theory and engineering from Harbin Engineering University, Harbin, China, in 2007.

He is currently a Professor with Yantai Research Institute, Harbin Engineering University. His research interests include power electronic converters, renewable energy generation, and wireless power transfer.